SCIENTIFIC REPORTS

OPEN

SUBJECT AREAS:
METALS AND ALLOYS
STRUCTURE OF SOLIDS AND LIQUIDS
MECHANICAL ENGINEERING
SURFACES, INTERFACES AND THIN FILMS

Received
28 October 2012

Accepted
7 December 2012

Published
8 January 2013

Correspondence and requests for materials should be addressed to X.L.M. (xlma@imr.ac.cn)

Local decomposition induced by dislocation motions inside precipitates in an Al-alloy

B. Yang, Y. T. Zhou, D. Chen & X. L. Ma

Shenyang National Laboratory for Materials Science, Institute of Metal Research, Chinese Academy of Sciences, Wenhua Road 72, 110016 Shenyang, China.

Dislocations in crystals are linear crystallographic defects, which move in lattice when crystals are plastically deformed. Motion of a partial dislocation may remove or create stacking fault characterized with a partial of a lattice translation vector. Here we report that motion of partial dislocations inside an intermetallic compound result in a local composition deviation from its stoichiometric ratio, which cannot be depicted with any vectors of the primary crystal. Along dislocation slip bands inside the deformed Al_2Cu particles, redistribution of Cu and Al atoms leads to a local decomposition and collapse of the original crystal structure. This finding demonstrates that dislocation slip may induce destabilization in complex compounds, which is fundamentally different from that in monometallic crystals. This phenomenon of chemical unmixing of initially homogeneous multicomponent solids induced by dislocation motion might also have important implications for understanding the geologic evolvement of deep-focus peridotites in the Earth.

Precipitate hardening and dispersion strengthening have been widely applied in many engineering materials, in which small particles of second phase (usually with complex crystal structure) play critical role in resisting dislocation motion in the matrix. In case of precipitate hardening, the hardness or yield strength of an alloy, which was experienced a higher temperature solution treatment, increases with the presence of small-sized precipitation and these precipitates usually have coherent or semi-coherent interface with the matrix. In contrast, in dispersion strengthening alloys, dispersed second phases usually do not have coherent interface with the matrix, such as Al_2O_3-reinforced Al composites. Quantity, morphology, and distribution of these small particles are of critical importance in tuning mechanical properties of the materials. However, in the past decades, more and more experimental observations indicate that the small-sized second phase can be decomposed during plastic deformation, leading to degradation of material properties. For instance, when Al-Cu alloys with θ' precipitate is plastically deformed at ambient temperature, dissolution or decomposition of the precipitates was detected[1,2]. Such a phase dissolution induced by plastic deformation has been observed in various Al-alloys in which precipitates play a crucial role in mechanical performance of the alloys, such as $Al_{13}Fe_4$ particle in Al-Fe[3], β'-phase in Al-Mg-Si[4], γ'-phase in Al-Ag[5], η'-phase in Al-Zn-Mg[6] and δ'-phase in Al-Li alloy[7,8]. In addition, steels provide another example where deformation-induced phase dissolution has been recognized for decades. When a pearlitic steel (consisting of cementite (Fe_3C) and ferrite) is plastically deformed at ambient temperature, Fe_3C particles are found to refine and dissolve[9–12], typically in heavily cold drawing of pearlitic steels for producing extraordinarily strong wires[13].

The dissolution of the strengthening particles in engineering alloys under mechanical loading unavoidably leads to a detrimental consequence in the designed microstructure and performance of the materials. Stability control of the strengthening particles relies on a thorough understanding of the mechanism of dissolution, in which the behavior of dislocations is believed to be the central issue. Interactions between dislocations and small particles have been extensively studied and several mechanisms have been proposed, such as Orowan mechanism[14–16] and cutting mechanism[17,18]. In addition, particular attention has been paid to the interface between second phase and matrix[9–11,19–22]. Although it is know that motion of partial dislocation in ordered structures may remove or create anti-phase boundaries, dislocation behaviors inside the precipitates with complex structures like those in Al-alloys are not well understood. Dislocation structure at atomistic scale (particularly at the core of a dislocation) is crystal structure-dependent. Hence, dislocation dynamics in complex structures may differ fundamentally from that in monometallic lattices.

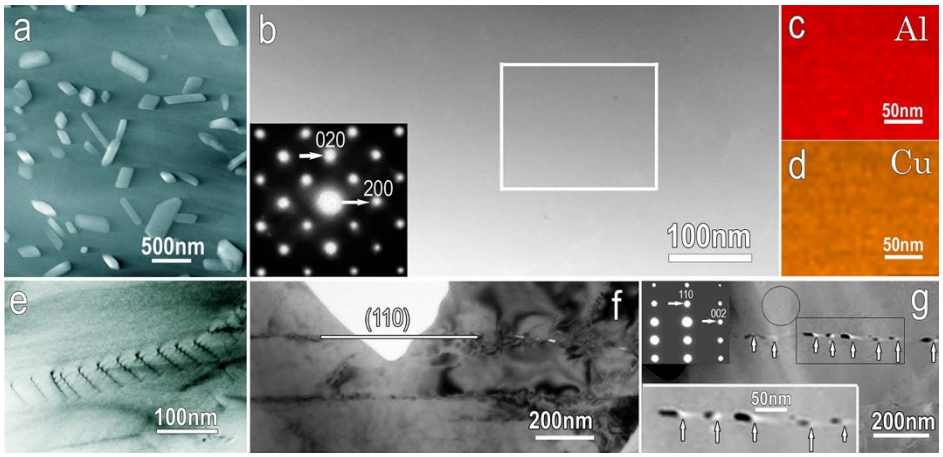

Figure 1 | (a) HAADF image showing the microstructural characteristics of the as-received dual-phase material. The particles embedded in Al matrix are tetragonal θ-Al_2Cu precipitates, verified by X-ray diffraction and a series of electron diffraction patterns. (b) HAADF image of an area within a single crystalline Al_2Cu precipitate along [001] crystallographic direction (see inset). (c) and (d) are elemental maps of Al and Cu, respectively, corresponding to the area squared in (b). Both Al and Cu are homogeneously distributed. (e) Micrograph showing an array of dislocations in the precipitate induced by deformation. (f) Bright-field TEM image showing slip bands on (110) crystallographic planes in an Al_2Cu particle. (g) HAADF image of the same area as that in (f) shows clear contrast variation along the slip band. The bottom-left inset is a section along this slip band marked with black rectangle. The up-left inset is an EDP of [1$\bar{1}$0] zone axis from the area marked with a black circle.

Results

We chose an Al-4wt.%Cu alloy in this study. The alloy experienced a solution treatment at 520°C followed by ageing at 300°C for 48 hours, as shown in Fig. S1. The as-received sample is composed of tetragonal θ-Al_2Cu precipitates embedded in Al matrix, Fig. 1a and Fig. S2. Each of the Al_2Cu precipitates is a single crystal, as confirmed by the homogeneous contrast of the high-angle-angular-dark-field (HAADF) image in TEM (Fig. 1b), as well as by the electron diffraction pattern (Inset in Fig. 1b). It is noted that HAADF images provide strong contrast associated with the local variety of chemical compositions and/or thickness contribution[23]. Elemental maps of Al and Cu in the single crystalline Al_2Cu (Fig. 1c, 1d) show

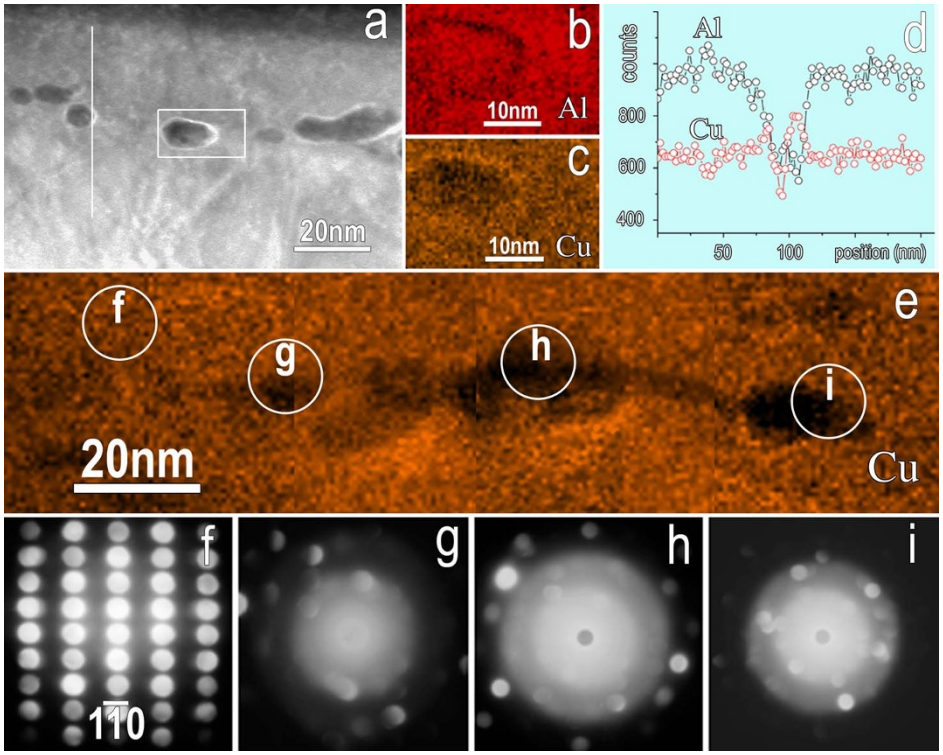

Figure 2 | (a) HAADF image of a section along a typical slip band. It is seen that the morphology of Cu-rich areas ranges from circular to elliptical, and sometimes irregular. (b) and (c) are Al and Cu maps, respectively, obtained from the area marked with a white rectangle in (a). A darker ring in (b) corresponding to the brighter ring in (c) is poor of Al and rich of Cu. (d) is EDS profiles showing the local composition fluctuation along the slip band. The scanning route for this EDS profile is perpendicular to the slip band marked with a white vertical line in (a). (e) Cu-map along the slip band, where the intensity of Cu is varied. (f) [1$\bar{1}$0] EDP taken in the area close to the slip band. (g–i) EDPs taken at different Cu-poor areas along the slip band. These EDPs can be no longer indexed to tetragonal Al_2Cu due to decomposition and structural collapse.

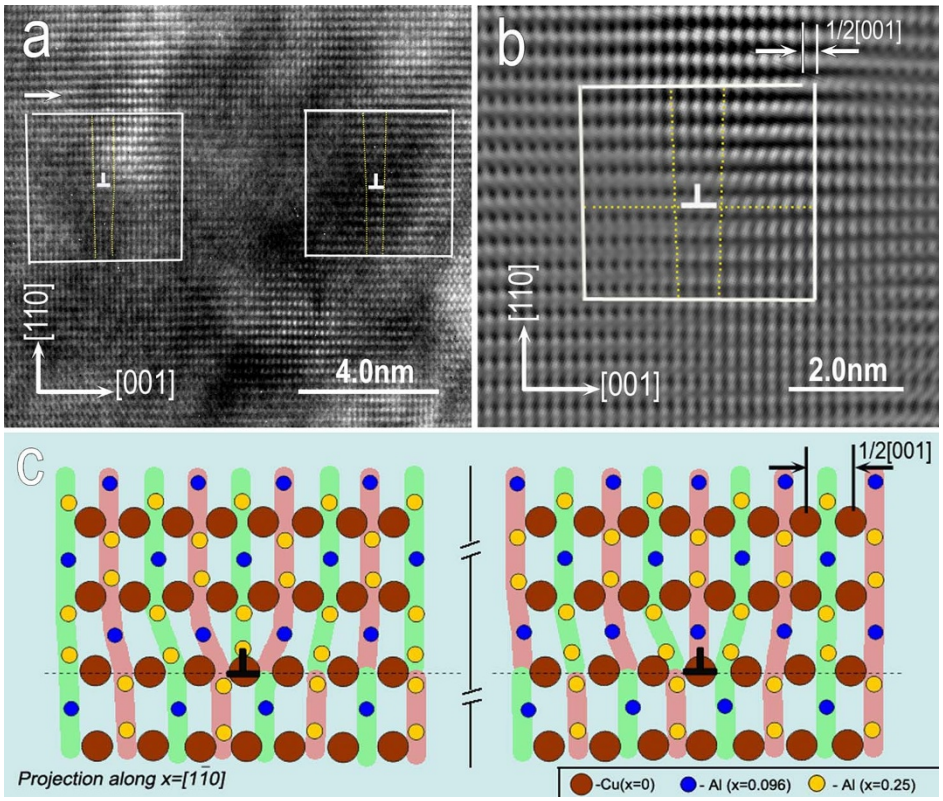

Figure 3 | (a) HREM image obtained from [1$\bar{1}$0] direction showing a dislocation array with a slip system [001](110). Burgers circuit is outlined for each dislocation, which exhibits the lattice displacement of 1/2[001] in this projection. (b) High magnification image of the partial dislocation (left partial in (A)). Stacking fault in the right of dislocation core ("⊥") is not resolved since the atomic projections of (001) and 1/2(001) planes are the same. (c) Atomic structural model of the partials viewed along the dislocation line. Here, atoms in three sub-layers (x = 0, 0.096, 0.25) are selected for projection in order to distinguish the two cores. The partial changes the stacking of the crystal (vertical direction in this schematic representation), i.e. it either removes or creates a stacking fault. The whole configuration of two partials and stacking fault (an ellipsis between two cores are marked) is called an extended dislocation.

a rather homogeneous distribution of both elements. Compositional fluctuations in the measured areas are within 65∼68 at% Al and correspondingly 31∼35 at% Cu.

Plastic deformation of the sample was performed by using the surface mechanical attrition treatment (SMAT) under vacuum of 6×10^{-2} Pa at liquid nitrogen temperature for 60 minutes with a vibrating frequency of 50 Hz. SMAT produces a gradient variation of plastic strain (and strain rate) in the treated surface layer[24–26]. The overall deformation layer in the SMAT sample is about 40 μm thick (Fig. S3), in which Al_2Cu particles at different depths from the treated surface are deformed with different plastic strains. TEM analysis indicates that, in addition to the Al matrix, Al_2Cu precipitates are also plastically deformed and strain-induced dislocations are observed inside the precipitates (Fig. 1e). Semi-quantitative X-ray diffraction analysis with a low scanning angle of 3° shows that the volume fraction of Al_2Cu precipitates in the topmost deformed layer (of about 2 μm thick) is reduced by 35.6% after SMAT (Fig. S4), indicating that a large volume of the precipitates has been dissolved as a result of heavy plastic deformation in the topmost layer.

In the deep deformed layer (30∼40 μm from the treated surface), presence of slip bands along (110) crystallographic plane inside the deformed Al_2Cu particles is one of the salient features, as seen in bright-field TEM images (Fig. 1f). HAADF image (Fig. 1g) of the same area as that in Fig. 1f shows that the contrast along the slip band is rather inhomogeneous (the most remarkable areas are up-ward arrowed). This signifies that the chemical composition along the slip band is deviated from that of unformed state. A close observation, as in the inset of Fig. 1g, reveals a more distinct contrast where each darker area is attached with a brighter elliptical domain.

Semi-quantitative characterization of the composition variations in a deformed Al_2Cu particle is performed by elemental mapping and X-ray energy dispersive spectrometer (EDS) analysis. Local areas with a contrast inhomogeneity along the slip band in the HAADF image are selected (Fig. 2a), with a particular attention to the Al and Cu distribution. The elemental maps of the area marked with a while rectangle in Fig. 2a are shown in Fig. 2b and 2c. In the Al map (Fig. 2b), a darker ring is observed. At the corresponding position, a ring with brighter contrast is seen in the Cu map (Fig. 2c). This means the ring area is poor of Al and rich of Cu. Such a Cu segregation leaves a Cu-poor area in its vicinity. Furthermore, EDS profiles (Fig. 2d) scanned along the vertical line in Fig. 2a also indicate that a composition fluctuation happened. The wavy counts indicate a remarkable jump of chemical compositions. Detailed statistic measurements from a dozen of EDS spectra indicate that the composition in the Cu-rich areas ranges within 38∼46 at% Cu and 53∼62 at% Al. This corresponds to Al/Cu ratio of 1.16∼1.63, deviated pronouncedly from the Al_2Cu stoichiometric ratio (2 : 1). By comparison of HAADF images and the corresponding EDS profiles, one may see that the area with a brighter HAADF contrast is always rich of Cu, while the darker area is poor of Cu. Such an elemental redistribution can be overviewed clearly in a Cu mapping (Fig. 2e), where Cu-rich and Cu-poor areas are alternately present along the slip band.

A series of electron diffraction experiments were carried out to identify the structural evolution in the area corresponding to the decomposition. For comparisons, the [1$\bar{1}$0] electron diffraction pattern (EDP) taken in the area close to the slip band is shown (Fig. 2f). It is interesting to note that when electron beam is shifted in a parallel approach to the Cu-poor areas along the slip band, the

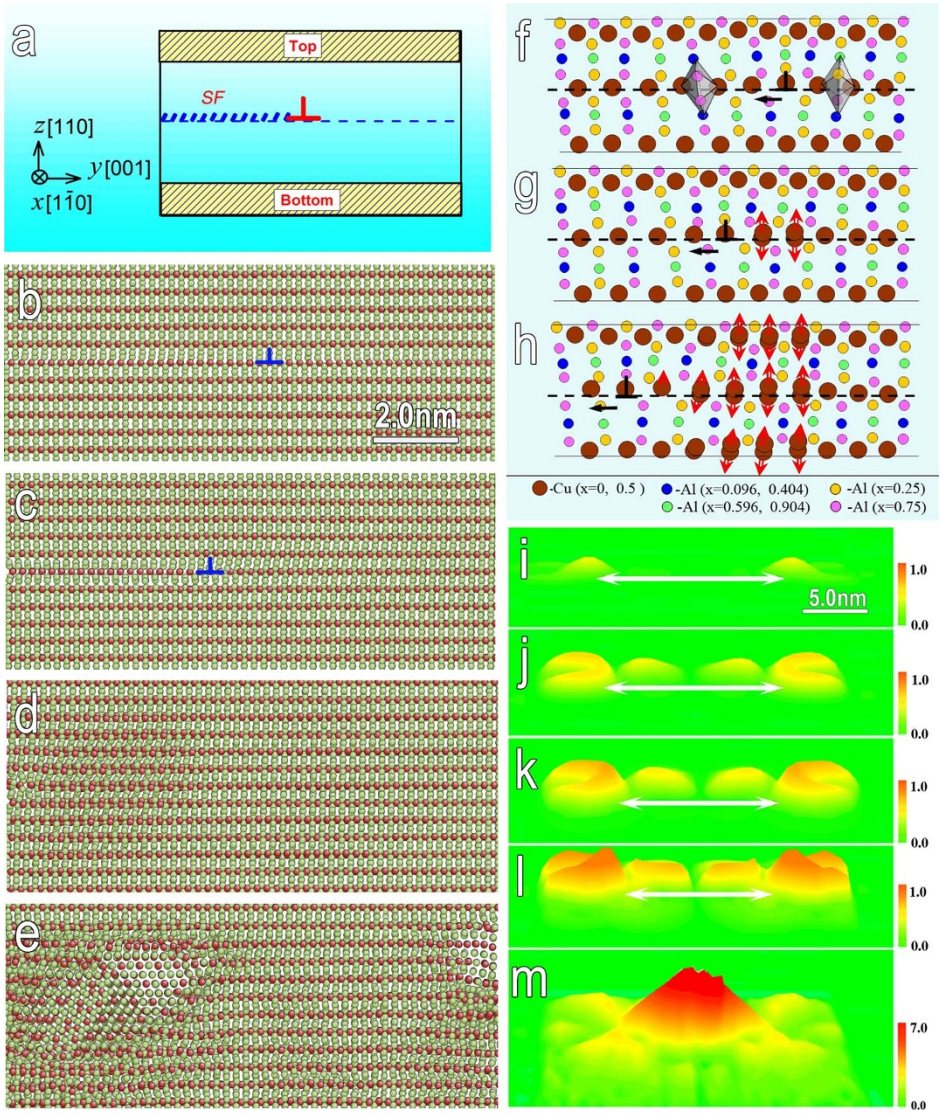

Figure 4 | (a) Schematic of the computational cell used for MD simulations. The dislocation is indicated with " ⊥ "; and the stacking fault area (in the left of the core) is also marked. (b) Cell for MD simulation, where partial dislocation is involved. (c–e) Snapshots of the atomic configuration at 14,000, 200,000, and 400,000 timesteps, respectively. In (b–e), the green spheres denote Al and the brown spheres Cu atoms, respectively. (f) Atomistic configurations projected along [1$\bar{1}$0] direction where perfect area, partial core, and stacking fault are represented. (g) and (h) show a continuous motion of dislocation leaves behind Cu displacements (red-arrowed) around the slip plane. (i–m) MD simulation indicates that the two partials tend to move toward each other (see the length changing of the double-arrowed bars in the figure). Colored according to the displacement values ($\sqrt{dx^2+dy^2+dz^2}$), the plots display an evolution of Cu displacement at 6,000, 10,000, 16,000, 30,000, and 240,000 timesteps, respectively. In (i–l), the displacement values are from 0 to 1 Å; while in (M) the range is 0∼7Å. The additional peaks between the two partials in (j, k, l) are believed to result from the local distortion under stress in the stacking fault area.

EDPs display completely different characteristics (Figs. 2g–2i). The EDPs can be no longer indexed to tetragonal Al_2Cu. In other words, dislocation motion along the slip band inside the Al_2Cu precipitate results in not only chemical decomposition but also a lattice structure collapse, which differs fundamentally from the scenario in monometallic crystals.

Discussion

Dislocation characteristics in the body-centered tetragonal Al_2Cu crystal have been studied earlier by diffraction contrast analysis and high-resolution imaging[27,28]. Dislocations with Burgers vectors of $\frac{1}{2}$<111>, [001], and [100] were identified, and faults on (110) and (00$\bar{1}$) planes were also observed. In our SMAT sample, dislocations associated with the slip system of [001](110) are frequently observed. High resolution imaging (Fig. 3a) indicates that such a dislocation is usually dissociated into two partial dislocations with a stacking fault in between. The separation distance between two partials is in a range of 10∼20nm. The left partial in Fig. 3a is magnified as seen in Fig. 3b, where a lattice displacement of $\frac{1}{2}$[001] can be identified in this projection. The tetragonal Al_2Cu crystal has eight sub-layers stacked along <110> direction, namely, $A_1B_1CB_2A_2B_2CB_1$ (schematically shown in Fig. S5). Aluminum atoms in layer "A" form a network of hexagons and the aluminum atoms in adjacent layer "B" is located above the hexagonal centers. Layer "C" constituted of copper atoms positioned between two "B-layer". The puckered "BAB" layers can be considered as a sandwich structure, and a gliding by 1/2[001] will result in the atoms in layer "B" move to the edges of hexagons of layer "A", which should be extremely unstable. Thus a slip should occur between "B" and "C" layers. Based on this reasoning, the core structure at each partial is proposed as shown in Fig. 3c, where atoms in three sub-layers are illustrated (an ellipsis is introduced in the stacking faults area between two cores).

Detailed molecular dynamical (MD) simulations were performed to the right partial in Fig. 3a in order to monitor atomistic processes during dislocation motion. In the computational cell used in MD simulations (Fig. 4a), the partial dislocation is created by removing two adjacent atomic half planes from the crystal structure (Fig. 4b). Under a stress, in Fig. 4a, the Top atoms are given a set velocity along y axis but the Bottom atoms are fixed. In this system, the generated stress propagates from the Top to the dislocation on the central plane. At the first stage of simulation, the dislocation is able to move with the help of stress on the slip plane (110) along [001] direction. The motion happens via shifting vertical rows of atoms relative to each other on the upper half of the slip plane. With an increasing of timesteps, stress-induced distortion becomes more and more severe from 14,000 (Fig. 4c), 200,000 (Fig. 4d), to 400,000 timesteps (Fig. 4e) where a localized Cu-segregation with "eyebrow-like" configuration emerges. Such a local lattice disorder can be also characterized by measuring the centrosymmetry parameter (Fig. S6). The maximum ratio of Cu quantity per unit volume ($Å^3$) in the Cu-rich to the Cu-poor areas in Fig. 4e gets to 2.5 approximately.

Stacking fault between two partial dislocations can be considered as a plate-like "precipitate", which establishes a new bonding length and changes the *d* spacings of planes parallel to the slip plane[29]. In other words, stacking fault in an extended dislocation results in a change of local mass density. In such a case, the motion of dislocation inside a complex compound may aggravate the lattice distortion. Once the atomistic displacement happens, it becomes more and more severe under stress until phase decomposition occurs via Cu segregation. On the basis of the MD simulations, a continuous development of atomistic configuration versus dislocation motion at an initial stage is schematically illustrated (Fig. 4f–h), where atoms in all the eight sub-layers are projected along $[1\bar{1}0]$ direction.

A computational cell with 22912 atoms was set up to monitor the motions of the extended dislocation (two partials are embedded in the cell). The MD simulation indicates that the equilibrium separation distance of the two partials is 14.4 nm after optimization. Similar to the simulations of one partial in Fig. 4a–e, Cu displacement on (110) plane becomes more and more remarkable with increasing the time-steps, seen in Fig. 4i–l which are colored according to the displacement values. In the meanwhile, the two partials tend to contract under a shear stress (double-arrowed bars in Fig. 4i–l), and finally combined together at 240,000 timesteps leaving a strip of Cu displacement (yellow together with red in Fig. 4m). The contraction of extended dislocations might lower their kinetic energies enough to offset the stacking fault energies that determine their extensions, as proposed theoretically for f.c.c crystals[30]. The dimension of such a Cu-displacement region is nearly the same as the distance between two partials prior to dislocation motion (schematically illustrated in Fig. S7). That is to say, the final degree of Cu segregation depends on the width of extended dislocation in real materials. The Cu displacements with maximum values (red in Fig. 4m) are believed to correspond to Cu-poor domains in Fig. 1 and Fig. 2.

Dislocations exist in various kinds of materials including metals, alloys, compounds, ceramics, and polymers. Our finding unambiguously demonstrates that dislocation motions in complex compounds may lead to decomposition and structural collapse around the slip planes, which differs fundamentally from that in monometallic systems. The spatial coupling of dislocation slip and compound dissolution is of significance in advancing our understanding of the processing-property relationship in materials, and also in optimizing mechanical properties of engineering materials by means of controlled plastic deformation processing.

Methods

An Al-4wt.%Cu alloy was selected and experienced a solution treatment at 520°C followed by ageing at 300°C for 48 hours, the as-received sample is composed of tetragonal θ-Al_2Cu precipitates embedded in Al matrix. X-ray diffractions at lower scanning angle of 3° were performed to determine phases in the 2 μm thick layer from the top. A Tecnai G^2 F30 transmission electron microscope, equipped with HAADF detector and X-ray dispersive spectrometer systems, was used at 300 kV for diffraction, HAADF imaging, and composition analysis. MD simulations with Large-scale Atomic/Molecular Massively Parallel Simulator (LAMMPS), are performed using the embedded atom method (EAM) interatomic potential.

1. Murayama, M., Horita, Z. & Hono, K. Microstructure of two-phase Al–1.7 at% Cu alloy deformed by equal-channel angular pressing. *Acta Mater.* **49**, 21–29 (2001).
2. Hutchinson, C. R. *et al*. Quantifying the strain-induced dissolution of precipitates in Al alloy microstructures using nuclear magnetic resonance. *Acta Mater.* **57**, 5645–5653 (2009).
3. Senkov, O. N. *et al*. Microstructure and microhardness of an Al-Fe alloy subjected to severe plastic deformation and aging. *Nanostruct. Mater.* **10**, 691–698 (1998).
4. Cabibbo, M., Evangelista, E. & Vedani, M. Influence of severe plastic deformations on secondary phase precipitation in a 6082 Al-Mg-Si alloy. *Metall. Mater. Trans. A* **36**, 1353–1364 (2005).
5. Horita, Z. *et al*. Achieving high strength and high ductility in precipitation-hardened alloys. *Adv. Mater.* **17**, 1599–1602 (2005).
6. Xu, C., Furukawa, M., Horita, Z. & Langdon, T. G. Influence of ECAP on precipitate distributions in a spray-cast aluminum alloy. *Acta Mater.* **53**, 749–758 (2005).
7. Lendvai, J., Gudladt, H. J. & Gerold, V. The deformation-induced dissolution of δ′ precipitates in Al-Li alloys. *Script Metall.* **22**, 1755–1760 (1988).
8. Berchet, Y., Louchet, F., Marchionni, C. & Verger-Gaugry, J. L. Experimental (TEM and STEM) investigation and theoretical approach to the fatigue-induced dissolution of δ′ precipitates in a 2.5 wt% Al-Li alloy. *Philos. Mag. A* **56**, 353–366 (1987).
9. Gavriljuk, V. G. Decomposition of cementite in pearlitic steel due to plastic deformation. *Mater. Sci. Eng. A* **345**, 81–89 (2003).
10. Languillaume, L., Kapelski, G. & Baudelet, B. Cementite dissolution in heavily cold drawn pearlitic steel wires. *Acta Mater.* **45**, 1201–1212 (1997).
11. Ivanisenko, Yu., Lojkowski, W., Valiev, R. Z. & Fecht, H. J. The mechanism of formation of nanostructure and dissolution of cementite in a pearlitic steel during high pressure torsion. *Acta Mater.* **51**, 5555–5570 (2003).
12. Zhou, L., Liu, G., Ma, X. L. & Lu, K. Strain-induced refinement in a steel with spheroidal cementite subjected to surface mechanical attrition treatment. *Acta Mater.* **56**, 78–87 (2008).
13. Embury, J. D. & Fisher, R. M. The structure and properties of drawn pearlite. *Acta Metall.* **14**, 147–159 (1966).
14. Orowan, E. Symposium Internal Sreesses in Metals and Alloys (*Institute of Metals,* London) 451–453 (1948).
15. Kelly, A. & Nicholson, R. B. Precipitation hardening. *Prog. Mater. Sci.* **10**, 151–391 (1963).
16. Bacon, D., Kocks, U. & Scattergood, R. The effect of dislocation self-interaction on the Orowan stress. *Philos. Mag.* **28**, 1241–1263 (1973).
17. Gleiter, H. & Hornbogen, E. Beobachtung der Wechselwirkung von Versetzungen mit kohärenten geordneten Zonen (II). *Phys. Stat. Sol. (b)* **12**, 251–264 (1965).
18. Gerold, V. & Haberkorn, H. On the critical resolved shear stress of solid solutions containing coherent precipitates. *Phys. Stat. Sol. (b)* **16**, 675–684 (1966).
19. Srolovitz, D. J., Petkovic-Luton, R. A. & Luton, M. J. Edge dislocation-circular inclusion interactions at elevated temperatures. *Acta Metall.* **31**, 2151–2159 (1983).
20. Gridnev, V. & Gavrilyuk, V. Cementite decomposition in steel under plastic deformation (a review). *Phys. Metals* **4**, 531–551 (1982).
21. Shabashov, V. A. *et al*. Deformation-induced phase transitions in a high-carbon steel. *Mater. Sci. Eng. A* **346**, 196–207 (2003).
22. Sauvage, X. & Ivanisenko, Y. The role of carbon segregation on nanocrystallisation of pearlitic steels processed by severe plastic deformation. *J. Mater. Sci.* **42**, 1615–1621 (2007).
23. Pennycook, S. J. Structure determination through Z-contrast microscopy. *Advances in imaging and electron physics* **123**, 173–206 (2002).
24. Lu, K. & Lu, J. Surface nanocrystallization (SNC) of metallic materials-presentation of the concept behind a new approach. *J. Mater. Sci. Tech.* **15**, 193–197 (1999).
25. Tao, N. R. *et al*. An investigation of surface nanocrystallization mechanism in Fe induced by surface mechanical attrition treatment. *Acta Mater.* **50**, 4603–4616 (2002).
26. Tong, W. P. *et al.* Nitriding iron at lower temperatures. *Science* **299**, 686–688 (2003).
27. Belgacem, C. H. *et al*. HRTEM observation of a <113> θ low angle tilt boundary in the Al–Al 2 Cu (θ) eutectic composite. *Phys. Stat. Sol. (a)* **189**, 183–196 (2002).
28. Bonnet, R. & Loubradou, M. Crystalline defects in a BCT Al2Cu (θ) single crystal obtained by unidirectional solidification along [001]. *Phys. Stat. Sol. (a)* **194**, 173–191 (2002).
29. Ferreira, P. J. & Müllner, P. A thermodynamic model for the stacking-fault energy. *Acta Mater.* **46**, 4479–4484 (1998).
30. Gilman, J. J. Contraction of extended dislocations at high speeds. *Mater. Sci. Eng. A* **319–321**, 84–86 (2001).

Acknowledgements

We thank Professor K. Lu for the critical comments on this work and Mr. X. Shi for his assistance in sample treatment and Mr. S. C. Wang for his assistance in X-ray diffraction.

This work is supported by the National Natural Foundation of China and Ministry of Science & Technology of China (2009CB623705).

Author contributions:

X.L.M. designed the overall study and wrote the paper. TEM experiments were performed by B.Y. and Y.T.Z. (equally contributed in the experiments). D.C. carried out the theoretical calculations. All authors contributed to the discussion of the data.

Additional information

Supplementary information accompanies this paper at http://www.nature.com/scientificreports

Competing financial interests: The authors declare no competing financial interests.

How to cite this article: Yang, B., Zhou, Y.T., Chen, D. & Ma, X.L. Local decomposition induced by dislocation motions inside precipitates in an Al-alloy. *Sci. Rep.* **3**, 1039; DOI:10.1038/srep01039 (2013).